# Rhombohedral Ordered Intermetallic Nanocatalyst Boosts the Oxygen Reduction Reaction

Xueru Zhao <sup>a,b</sup>, Hao Cheng <sup>d</sup>, Liang Song <sup>a</sup>, Lili Han <sup>d</sup>, Rui Zhang <sup>d</sup>, Gihan Kwon <sup>c</sup>, Lu Ma <sup>c</sup>, Steven Ehrlich <sup>c</sup>, Anatoly I. Frenkel <sup>a,e</sup>, Jing Yang <sup>b,\*</sup>, Kotaro Sasaki <sup>a,\*</sup>, Huolin L. Xin <sup>d,\*</sup>

#### **Abstract**

Low platinum-group-metal (PGM) ordered intermetallic catalysts have been considered one of the most promising candidates for catalyzing the oxygen reduction reaction (ORR) in fuel cells, but achieving the desired performances in terms of activity, durability and cost is still a grand challenge for the fuel cell research field. While the cubic- and tetragonal-ordered (L12 and L10 phases) low-PGM nanocatalysts have been investigated extensively and have shown considerably improved durability and activity toward the ORR, so far little is known about rhombohedral-ordered L11 catalysts. We report the synthesis of a L1<sub>1</sub>-ordered PtCu catalyst for the ORR. We demonstrate that, by applying nitrogen (N)-doping through a thermal treatment in an NH<sub>3</sub> gas, the activity and stability of the N-doped, rhombohedral ordered PtCu catalyst can be further enhanced, and the ORR mass and specific activities achieve nearly 5-fold and 4-fold enhancement in acidic media, respectively, relative to those of commercial Pt/C. In situ synchrotron X-ray absorption and pair-distribution-function measurements reveal that both the formation of the ordered intermetallic structure and N-doping synergistically improve the corrosion resistance of the PtCu catalyst by lowering the Cu diffusivity, and introduce a compressive strain effect regulating the adsorption of oxygenated species on the Pt surface, thus accounting for the improved ORR kinetics.

Keywords: Oxygen reduction reaction, rhombohedral ordered intermetallics, core shell, N doping, PtCu nanocatalyst

<sup>&</sup>lt;sup>a</sup> Chemistry Division, Brookhaven National Laboratory, Upton, NY, 11973, USA

<sup>&</sup>lt;sup>b</sup> Institute of New-Energy Materials, Key Laboratory of Advanced Ceramics and Machining Technology of Ministry of Education, School of Materials Science and Engineering, Tianjin University, Tianjin, 300072, China

<sup>&</sup>lt;sup>c</sup> National Synchrotron Light Source II, Brookhaven National Laboratory, Upton, NY, 11973, USA.

<sup>&</sup>lt;sup>d</sup> Department of Physics and Astronomy, University of California, Irvine, CA, 92697, USA

<sup>&</sup>lt;sup>e</sup> Department of Materials Science and Chemical Engineering, Stony Brook University, Stony Brook, NY, 11794, USA

<sup>\*</sup> Correspondence should be addressed to <a href="https://huolinx@uci.edu">huolinx@uci.edu</a> (H. L. Xin), <a href="https://ksasaki@bnl.gov">ksasaki@bnl.gov</a> (K. Sasaki), and <a href="https://yang.jing@tju.edu.cn">yang\_jing@tju.edu.cn</a> (J. Yang)

#### Introduction

As an alternative to internal combustion engines, proton exchange membrane fuel cells (PEMFCs) have received increasing attention due to their high energy conversion efficiency and their commercial potential in medium- and heavy-duty vehicle applications.<sup>1-4</sup> However, the performance of PEMFCs is limited by the sluggish kinetics of the oxygen reduction reaction (ORR) for the cathodes. So far, the widespread commercialization of PEMFCs is still thawted by the high cost of Pt.5-7 Therefore, developing highly efficient and stable electrocatalysts with low loading of Pt group metals (PGM) is of great significance. In this respect, many strategies have been pursued to improve low-PGM catalysts' ORR activity, including adopting thin Pt-shell on core structures,8-11 alloying/dealloying,12-14 shape control, <sup>15-17</sup> and forming ordered intermetallic Pt-M<sub>3d</sub> (M = 3d transition metals) phases. <sup>18-24</sup> Among them, structurally ordered low-PGM catalysts, in particular the cubically ordered L1<sub>2</sub> phase and the tetragonally ordered L1<sub>0</sub> phase, have been extensively investigated in the past years because of the availability of multiple degrees of freedom, such as ligand, linear and shear strains as well as the pure-Pt-shell thickness, 25 to tune their activity and durability toward the ORR.<sup>26-32</sup> For instance, L1<sub>2</sub>-ordered Pt<sub>3</sub>Co,<sup>33</sup> Pt<sub>3</sub>Cr<sup>34</sup> and L1<sub>0</sub>-ordered PtCo,<sup>18</sup> PtFe<sup>35</sup> exhibit enhanced ORR activity and durability than disordered alloy phases. Moreover, anion doping, such as nitrogen (N), could be used to further optimize the ligand and strain effects in low-PGM catalyst by forming the stable metal-N bonding, modifying the adsorption energetics of oxygenated species on the Pt surface, and in turn, improving the ORR activity and stability of electrocatalysts. 9, 36-37 As an example, our recent experimental analysis and the DFT calculations indicated that the M-N (M = Fe, Co, Ni) core could enhance the ORR performance of PtMN catalysts by inducing both the geometric and electronic effects on the Pt shells.9 On the other hand, the ORR performance of ordered intermetallic Pt<sub>x</sub>M<sub>y</sub> catalysts can be further improved by precisely tuning particle size and shape via controlling composition and synthesis conditions. 18, 38-39

Even though promising, most of the past work on ordered Pt- $M_{3d}$  catalysts are based on the  $L1_2$  and  $L1_0$  ordered phases and so far, there are few reports about the use of the rhombohedral order  $L1_1$  structure which is available to the low-temperature phase of

PtCu.<sup>40-41</sup> Because the L1<sub>1</sub> ordering is composed of alternating stacking of Pt and Cu close-packed (111)<sub>fcc</sub>/(001)<sub>ccp</sub> planes, it is reasonable to hypothesize that the PtCu catalyst favors Pt-terminated (111)<sub>fcc</sub>/(001)<sub>ccp</sub> whose ORR kinetics is influenced by the compressive strain and the ligand effect of Cu underneath.

To prove these hypotheses, herein, we have synthesized a L1<sub>1</sub>-ordered PtCu ORR catalyst supported on Ketjenblack (KB) (denoted as Int-PtCu/KB). Even the activity of Int-PtCu/KB is much higher than that of Pt/C, but both activity and durability of this catalyst can be further improved by the N-doping. The N-doped Int-PtCu/KB catalyst (denoted as Int-PtCuN/KB) exhibit a mass activity (MA) of 1.15 A mg<sub>Pt</sub><sup>-1</sup> and specific activity (SA) of 1.81 mA cm<sup>-2</sup> at 0.9 V, which increase 5.2 and 3.9 times compared with those of a commercial Pt/C catalyst, respectively. The ordered Int-PtCuN/KB catalysts also show significant improvement of the ORR durability in an acidic electrolyte. The *in situ* synchrotron measurements, *i.e.* X-ray absorption spectroscopy (XAS) and X-ray diffraction (XRD) coupled with the atomic pair distribution function (PDF) analysis, and atomic-resolution scanning transmission electron microscopy (STEM) imaging reveal in detail the formation of intermetallic structure and chemically stable Cu-N bonding in the PtCu core, which protect Cu from corrosion in acidic media, thereby leading to enhanced catalyst durability. We also show that the improved activity of Int-PtCuN/KB is due to the additional compressive strain provided by N-doping in the Cu sites.

#### **Results and discussion**

The low-magnification high angle annular dark-field STEM (HAADF-STEM) image in Figure 1a shows that the Int-PtCuN nanoparticles are highly dispersed on the KB support, and the average size is around 3.9 nm (derived from the inset of Figure 1a). The disordered PtCu (denoted as D-PtCuN/KB) nanoparticles synthesized by annealing in an NH3 gas at 500 °C show an average size of ~ 2.3 nm (Figure S1); the Int-PtCuN/KB was synthesized by applying an additional annealing to the D-PtCuN/KB at 800 °C in H2/Ar, and the slightly larger particle size of the Int-PtCuN/KB is caused by the additional thermal process to form the ordered phase. On the other hand, the Int-PtCu/KB sample synthesized by annealing in a

H<sub>2</sub>/Ar at 800 °C exhibits a similar particle distribution with an average size of around 3.8 nm (Figure S1), illustrating that N-doping has little effect on the particle size of catalysts. The synthesis methods for Int-PtCuN/KB, D-PtCuN/KB, and Int-PtCu/KB are simple and facile, as described in detail in Supporting Information (SI). In the XRD patterns displayed in Figure 1b, the peak positions of as-synthesized D-PtCuN/KB can be well indexed to (111), (200), (220), and (311) facets of a face-centered cubic (fcc) structure according to PDF #48-1549; meanwhile the characteristic diffraction peaks of Int-PtCuN/KB (Figure 1b and Figure S2a) and Int-PtCu/KB (Figure S2a) match well with an ordered intermetallic *R-3m* rhombohedral Pt<sub>1</sub>Cu<sub>1</sub> structure (PDF #42-1326), *i.e.* the rhombohedral ordered L1<sub>1</sub> phase, indicating the successful transition from disordered to the ordered L1<sub>1</sub> structure. By using the X-ray spectrum techniques, the uniform chemistry distributions evidence the successful doping of N atoms into the Int-PtCuN/KB nanoparticle, as shown in Figures 1c-h. The Pt:Cu mole ratio of Int-PtCuN/KB is almost 1:1 as confirmed by the EDS results (Table S1).

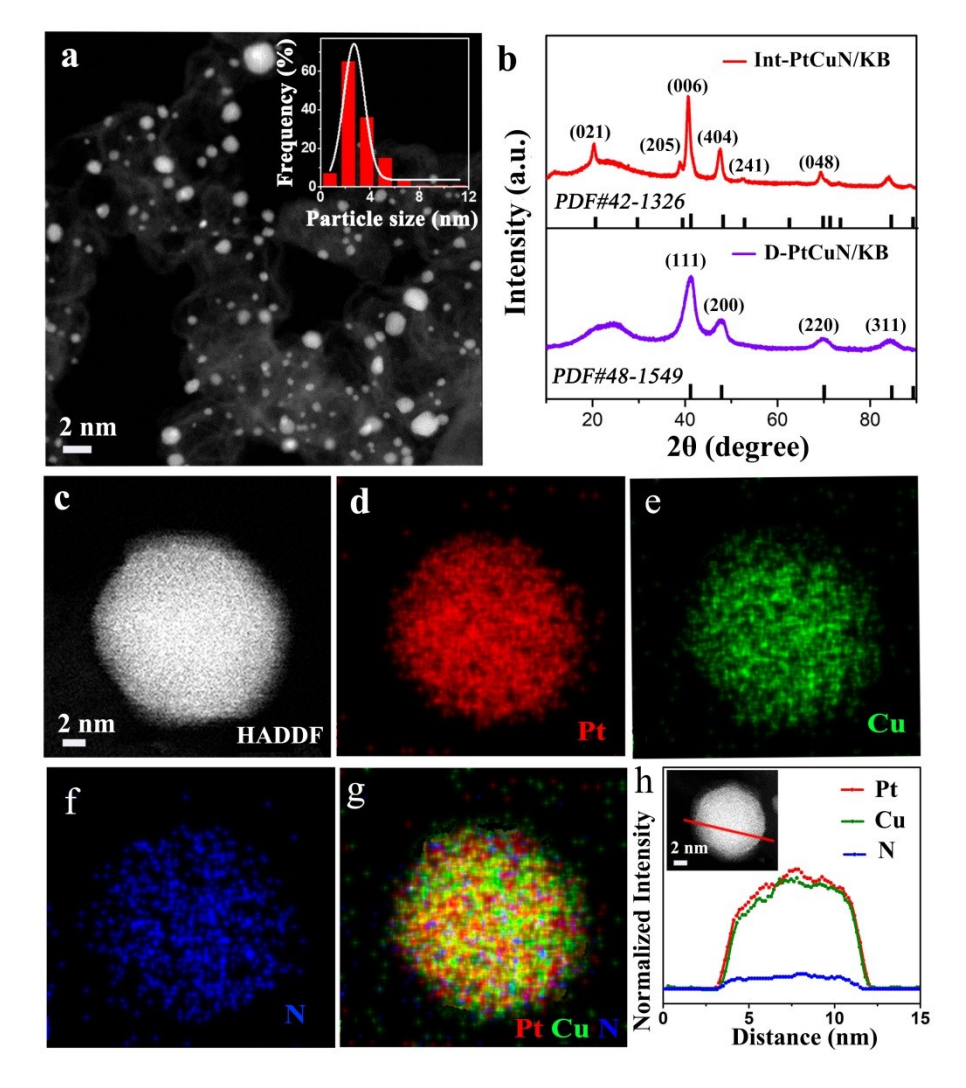


**Figure 1.** (a) HADDF-STEM image and the corresponding size distribution (inset) of the Int-PtCuN/KB nanoparticles. (b) XRD patterns of Int-PtCuN/KB and D-PtCuN/KB. The peak positions of the vertical black lines are corresponding to intermetallic PtCu (PDF #42-1236) and alloy PtCu (PDF #48-1549). (c-g) HADDF-STEM image and the energy dispersive X-ray spectroscopy (EDS) elemental mappings of the Int-PtCuN nanoparticle. (h) The EDS elemental line scanning image across a single Int-PtCuN particle.

The atomic-resolution HAADF-STEM image directly visualizes the atomic structure of the ordered intermetallic Int-PtCuN/KB catalysts. As shown in Figure 2a and Figure S2b, the lattice spacing from the HAADF-STEM image of a single particle are calculated to be 0.436 nm and 0.23 nm, which correspond to the (021) and (205) planes of the intermetallic PtCu, manifesting that the Int-PtCuN/KB nanoparticles prepared have an ordered intermetallic *R-3m* rhombohedral L1<sub>1</sub> structure. To study the explicit structure at atomic scale, the enlarged view of atomic-resolution HADDF-STEM image verifies that the ordered intermetallic structure of Int-PtCuN/KB is formed with a core comprising alternative layers of Pt and Cu

and a shell being a Pt monolayer (Figure 2b). As can be seen from Figure 2c, the simulated HAADF-STEM image agrees with the experimental image in Figure 2b. Figure 2d proposes the atomic model of disordered and ordered PtCu structures for better exhibition of the generation of the ordered structure as well as explanation of its behavior in the ORR process. The monolayer Pt shell is believed to efficiently protect Cu against acid etching from the ordered PtCu core during electrochemical potential cycling, resulting in improving the stability of electrocatalysts, as discussed below.

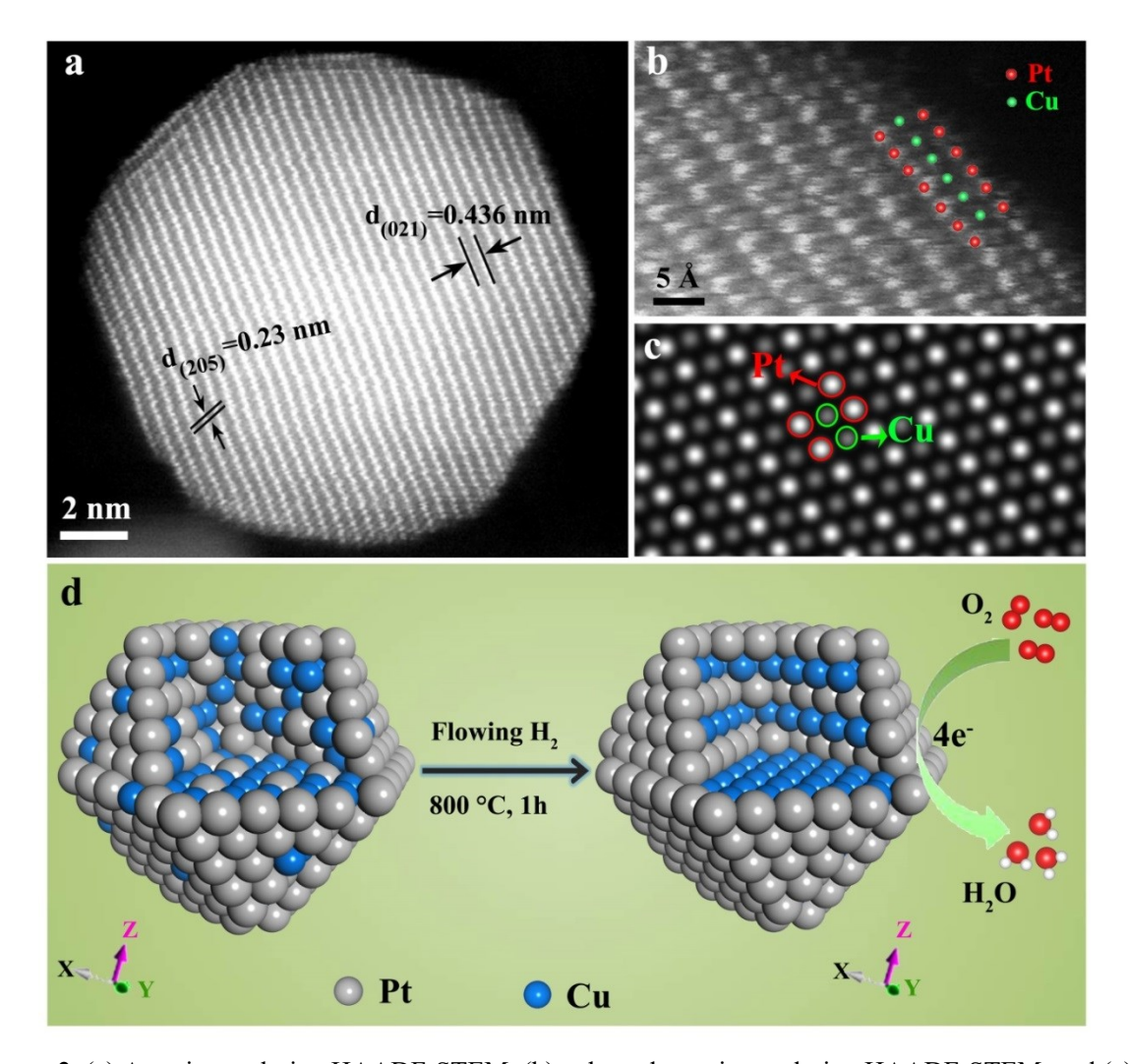


**Figure 2.** (a) Atomic-resolution HAADF-STEM, (b) enlarged atomic-resolution HAADF-STEM, and (c) simulated HAADF-STEM images of a single ordered Int-PtCuN particle. (d) The atomic model of disordered PtCu (left) and ordered PtCu (right), and a schematic diagram of the ORR on the ordered intermetallic PtCu model.

As presented in Figure 3a, the ORR performance of as-prepared Int-PtCuN/KB, Int-PtCu/KB, and D-PtCuN/KB catalysts was evaluated by polarization curve measurements in an O<sub>2</sub>-saturated 0.1 M HClO<sub>4</sub> electrolyte. Also shown is the result from a commercial Pt/C catalyst for comparison. The half-wave potential ( $E_{1/2}$ ) of the Int-PtCuN/KB catalyst is 916 mV (Table S2), which is higher than those of Int-PtCu/KB (904 mV), D-PtCuN/KB (889 mV), and commercial Pt/C (867 mV), illustrating that the ORR kinetics of the Int-PtCuN/KB catalyst is dramatically enhanced. The Koutecký-Levich (K-L) plots were derived from the rotating disk electrode (RDE) data (Figure 3b), and the electron-transfer number of Int-PtCuN/KB was calculated to be nearly 4.0, indicating a minimal peroxide formation.

Cyclic voltammetry (CV) was also employed to evaluate other electrochemical properties of as-obtained catalysts in an Ar-saturated 0.1 M HClO<sub>4</sub> electrolyte (Figure S3a). The electrochemical surface area (ECSA), which was obtained by the underpotentially adsorbed hydrogen (Hupd) method, increases in the following order, Int-PtCuN/KB (63.7 m<sup>2</sup>  $g^{-1}$ ) > Int-PtCu/KB (57.8 m<sup>2</sup> g<sup>-1</sup>) > D-PtCuN/KB (52.3 m<sup>2</sup> g<sup>-1</sup>) > Pt/C (47.6 m<sup>2</sup> g<sup>-1</sup>), as is seen in Table S2. The measures ECSA results for the Int-PtCuN/KB via CO stripping (Figure S3b) and the H<sub>upd</sub> method show clear differences (87.0 vs. 63.7 m<sup>2</sup> g<sup>-1</sup>), which is high possible induced by the suppression effect of sublayer Cu on the H<sub>upd</sub> and the formation of a "Pt skin" over the PtCu core. 42 After normalizing to Pt loading and the ECSA of Pt, the MA and SA of these catalysts can be obtained from the polarization curves, respectively. As revealed in Figure 3c, the MA and SA increase in the same order of Int-PtCuN/KB > Int-PtCu/KB > D-PtCuN/KB > Pt/C. Notably, the Int-PtCuN/KB catalyst shows a MA of 1.15 A mg<sub>Pt</sub><sup>-1</sup> and a SA of 1.18 mA cm<sup>-2</sup> at 0.9 V, which are respectively 5.2 times and 3.9 times higher than those of commercial Pt/C (0.22 A mg<sub>Pt</sub><sup>-1</sup>, 0.46 mA cm<sup>-2</sup>), and outperform some recently published literature about the ordered Pt-based intermetallic catalysts (Table S3). As we expected, both of the ordered Int-PtCuN/KB and Int-PtCu/KB catalysts exhibit higher performance than D-PtCuN/KB, suggesting that the formation of ordered intermetallic structure gives rise to optimized adsorption of oxygen species (O\*, OH\*, etc.) on the Pt surface, 35, 43 and therefore the improved activity for the ORR. Moreover, the MA and SA of Int-PtCuN/KB are higher than those of Int-PtCu/KB, suggesting that the N-doping can further enhance the activity of Int-PtCu catalysts towards the ORR.

To evaluate the electrocatalytic long-term durability, the as-prepared catalysts were examined by performing accelerated potential cycling from 0.6 to 0.95 V in a 0.1 M HClO<sub>4</sub> solution. After accelerated durability test (ADT), the H adsorption/desorption regions in the CV curves from the Int-PtCuN/KB barely changed as shown in the inset of Figure 3d, and the drop in ECSA of Int-PtCuN/KB is only 6.6 % after 20,000 ADT cycles (Table S4), which is much lower than those observed for Int-PtCu/KB, D-PtCuN/KB, and Pt/C (11.1 %, 9.2 %, and 25.6%, respectively). Meanwhile, the polarization curves of Int-PtCuN/KB displayed only a 9 mV negative shift of its  $E_{1/2}$  after 20,000 ADT cycles (Figure 3d). Conversely, Int-PtCu/KB, D-PtCuN/KB, and Pt/C showed 18, 27 and 12 mV negative shifts (Table S5), respectively, demonstrating that Int-PtCuN/KB exhibits the best long-term stability. The MA and SA losses of Int-PtCuN/KB at 0.9 V before and after the ADT are presented in Figure 3e. The MA and SA of Int-PtCuN/KB dropped only by 23.5 % and 18.2 % after 20,000 ADT cycles (Table S3), respectively, compared with those before the ADT test. In contrast, the D-PtCuN/KB catalyst exhibited MA and SA losses of 47.5 % and 42.5 % after 20,000 ADT cycles (Figure S4 and Table S5), demonstrating that the phase transformation from the disordered to ordered intermetallic structure improved the ORR durability considerably. In addition, the degradation of MA on the Int-PtCuN/KB catalyst (23.5 %) is much lower than that of Int-PtCu/KB (39.5 %), suggesting that the N-doping also has significantly improved the stability of the catalyst. As clearly shown in the MA comparison (Figure 3f), the Int-PtCuN/KB achieves the best durability in all the catalysts examined. The HAADF-STEM image and EDS mapping of Int-PtCuN/KB after 20,000 ADT cycles also indicate that a significant amount of Cu still remains in the core of Int-PtCuN/KB nanoparticles (Figure S5), further confirming that the monolayer Pt shells effectively protect the catalysts against Cu leaching from the nanoparticles in the acid media, thereby improving the ORR stability of the Int-PtCuN/KB catalyst. The results showed that the ORR activities and the stability of Int-PtCu/KB are higher than those of D-PtCuN/KB; this indicates that the formation of the ordered intermetallic structure might individually contribute more to the improvement of ORR performance than N-doping for this system. We emphasize that our approach by combining the two features (i.e., structural ordering and N-doping) can further enhance the ORR performance synergistically as demonstrated by the Int-PtCuN/KB catalyst. More

evidence for the excellent stability as well as the information about structural properties of the electrocatalyst at ORR-relevant potentials can be obtained by *in situ* XAS.

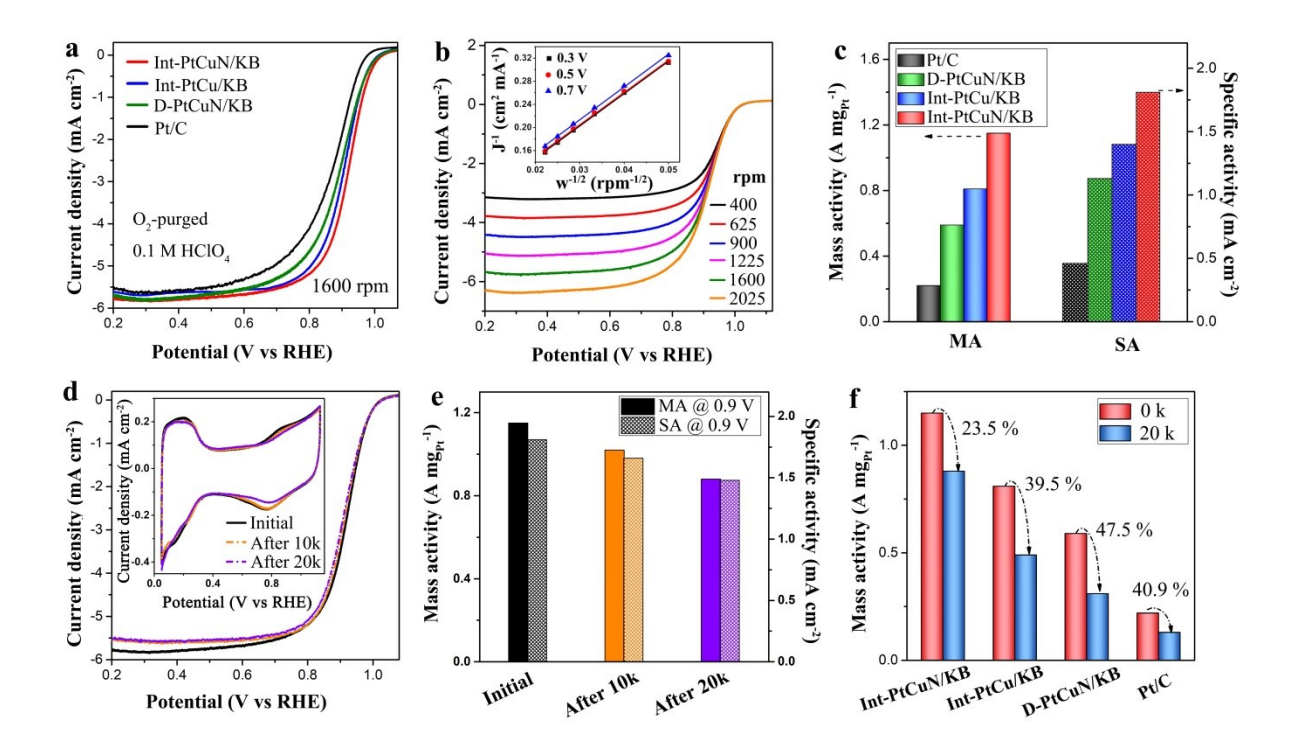


**Figure 3.** (a) ORR polarization curves of Int-PtCuN/KB, Int-PtCu/KB, D-PtCuN/KB, and commercial Pt/C in O<sub>2</sub>-saturated 0.1 M HClO<sub>4</sub> with a scanning rate of 10 mV s<sup>-1</sup>. (b) ORR polarization curves and Koutecky-Levich plots at different potential (inset) for Int-PtCuN/KB catalyst at various rpm. (c) Specific activity and mass activity of Int-PtCuN/KB, Int-PtCu/KB, D-PtCuN/KB, and commercial Pt/C at 0.9 V. (d) ORR polarization and CV (inset) curves of Int-PtCuN/KB catalyst before and after 20,000 ADT cycles. (e) Specific activity and mass activity of Int-PtCuN/KB catalyst at different ADT cycles. (f) The MA comparison of different samples before and after 20,000 ADT cycles.

The Cu K-edge X-ray absorption near edge structure (XANES) spectra of Int-PtCuN/KB at various potentials and the references (Cu foil and CuO) are displayed in Figure 4a. The significant changes in XANES of Int-PtCuN/KB with respect to the Cu foil and CuO imply that the local atomic environment and electronic state of Cu in Int-PtCuN/KB has been changed in comparison with the references. When the applied potential increases from 0.42 V to 1.12 V, only the main peak (around E = 8993 eV) of Cu K-edge XANES shifts very slightly towards the high energy with the increase potential (the inset in Figure 4a), which is likely caused by the oxidation of Cu. Moreover, Figure S6a presents the Fourier transform (FT) magnitude of  $k^2$ -weighted extended X-ray absorption fine structure (EXAFS) spectra of

the Cu K-edge of Int-PtCuN/KB; the peaks around 1.5 Å (uncorrected for the photoelectron phase shift) reflect the formation of Cu-O pairs. Compared to the Int-PtCu/KB (Figure S8) and D-PtCuN/KB (Figure S9), much less changes in the peak shapes in XANES and the Cu-O bond in FT-EXAFS of Int-PtCuN/KB are seen during the potential increasing from 0.42 V to 1.12 V, which indicates significant suppression of Cu oxidation for the Int-PtCuN/KB catalyst. Figure 4c shows more clearly the effect of applied potentials on the Cu oxidation, which was obtained by the linear combination fitting (LCF) to determine the fraction of Cu of Int-PtCuN/KB at 0.42 V (at a double layer region) and CuO from the XANES at a series of potentials. The percentages of the respective components in the sample can be given by the LCF using reference spectra.<sup>44</sup> As a fitting example, the Cu K-edge XANES spectra (Figure S7a) at 1.12 V together with those of an oxide-free spectrum at 0.42 V and CuO oxide reference are shown. We ascribe the origin of suppression of Cu oxidation to some or all of the following possibilities: (i) the generation of well-integrated Pt monolayer shells for Int-PtCuN/KB, thereby protecting the Cu from being dissolved in the acid electrolyte, (ii) the presence of ordered intermetallic structure, which has intrinsic corrosion-resistance, and (iii) the formation of chemically stable Cu-N bond, which effectively enhances the corrosion-resistance.

The *in situ* Pt L<sub>3</sub>-edge XANES spectra of Int-PtCuN/KB reflect a change in metallic state of Pt at different potentials, as depicted in Figure 4b. The white line (*i.e.* the main absorption peak) intensity of Int-PtCuN/KB increases with elevated potentials, due to the depletion of Pt's *d*-band caused by the formation of Pt oxide. The peaks around at 1.6 Å in FT-EXAFS of Int-PtCuN/KB also reflect the formation of Pt oxide (Figure S6b). We emphasize that commercial Pt/C shows much higher rises in white line intensity (Figure S10a) and peak intensity of Pt-O bond at 1.6 Å (Figure S10b) with increasing potentials than those in Int-PtCuN/KB (Figure 4b and 4f), Int-PtCu/KB (Figure S8d and S8e), and D-PtCuN/KB (Figure S9d and S9e), indicating that the Pt oxidation on these catalyst surfaces is prohibited. We note that the degree of potential dependence calculated from Int-PtCuN/KB is slightly larger than those from Int-PtCu/KB and D-PtCuN/KB (Figure 4d) obtained from the LCF of Pt L<sub>3</sub>-edge XANES spectra (Figure S7b); the order is Int-PtCuN/KB > Int-PtCu/KB > D-PtCuN/KB, which is the same order as that of the ECSAs obtained from the CVs. It is

likely that more Pt active sites are present on the Int-PtCuN/KB surface than the Int-PtCu/KB and D-PtCuN/KB surfaces during the ORR process.

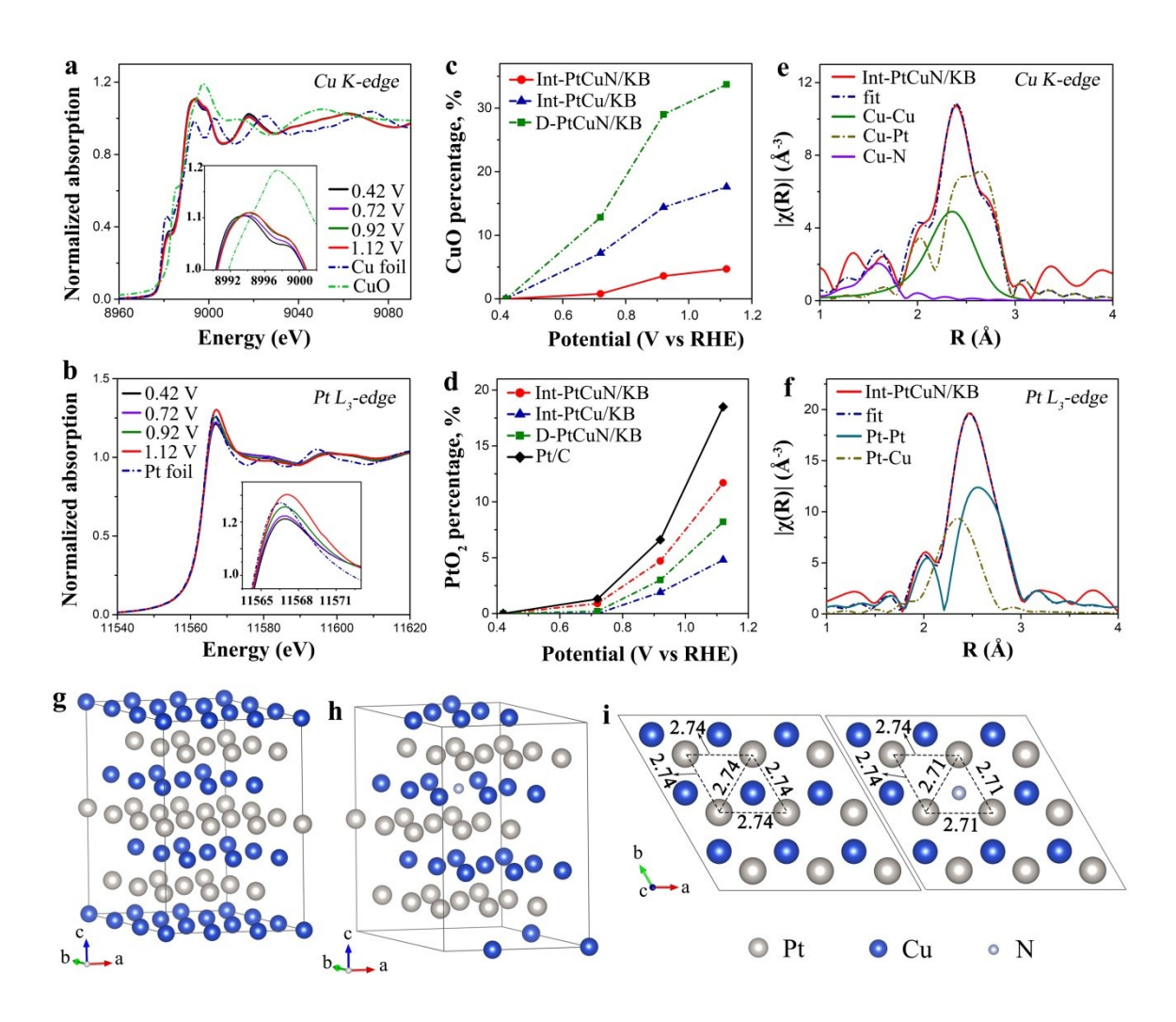


**Figure 4.** (a) Cu K-edge XANES spectra of Int-PtCuN/KB at a series of applied potentials, with Cu reference foil and CuO standard. (b) Pt L<sub>3</sub>-edge XANES of Int-PtCuN/KB at a series of applied potentials, with Pt reference foil. (c) Comparison of CuO percentage per Cu atoms in Int-PtCuN/KB, Int-PtCu/KB and D-PtCuN/KB with increasing potentials. (d) Comparison of PtO<sub>2</sub> percentage per Pt atoms in Int-PtCuN/KB, Int-PtCu/KB, D-PtCuN/KB and Pt/C with increasing potentials. (e) Cu K-edge FT-EXAFS spectrum of Int-PtCuN/KB at 0.42 V and the corresponding fitting curves (k²-weighting and k-range from 2.0 to 14.0 Å<sup>-1</sup> were used in Fourier transforms), and (f) Pt L<sub>3</sub>-edge FT-EXAFS spectrum of Int-PtCuN/KB at 0.42 V and the corresponding fitting curves (k²-weighting and k-range from 3.0 to 13.0 Å<sup>-1</sup> were used in Fourier transforms). (g) Crystallographic structure of the ordered intermetallic PtCu, and (h) ordered intermetallic PtCu with a N atom substituted a Cu site. (i) The changes of Pt-Pt bond length of the ordered intermetallic PtCu before (left) and after (right) N substitution.

EXAFS data analysis was performed for each element (Cu and Pt) concurrently, by

applying several constraints to the heterometallic (Cu-Pt) path parameters.  $^{47-48}$  The details about the fitting procedure are given in the su. Figure 4e and 4f show the Cu K-edge and Pt L<sub>3</sub>-edge EXAFS data of the Int-PtCuN/KB catalyst at 0.42 V and the corresponding fitting curves, respectively. For comparison, the data and fits of Int-PtCu/KB and D-PtCuN/KB are displayed in Figures S8c and S8f and Figures S9c and S9f, respectively. All the fits are in good agreement with the experimental spectra. The Pt-Pt coordination number (*CN*) of Int-PtCuN/KB is determined to be  $6.7 \pm 0.4$  (Table S6), which is very similar to those of Int-PtCu/KB ( $6.9 \pm 0.6$ , Table S7), and D-PtCuN/KB ( $6.4 \pm 0.6$ , Table S8). Comparing these results with those predicted for ideal models of cubic (fcc) and rhombohedral nanoparticles, we note that the CN of 6 corresponds a monolayer shell of Pt atoms residing in (111) surface planes. Previous observations of catalysts having Pt monolayer (ML) shells on their surfaces were discussed in detail elsewhere.  $^{37, 49-50}$  We note that, within the limits of the accuracy in CN determination, we are unable to discriminate between the intermetallic and disordered structures in this work, using EXAFS only. This emphasizes the importance of the correlated, multimodal approach for studying these materials.

Another marked observation is that the Pt-Pt bond distance of Int-PtCuN/KB (2.693 Å) is shorter (the change is outside the experimental error bars, Tables S5 and S6) than that of Int-PtCu/KB (2.701 Å), indicating that the N dopants induce a contraction in Pt bonding. Our recent study of N-doped intermetallic PtNi/KB catalysts (Int-PtNiN/KB) demonstrated that doped N atoms can be interstitially sited at a center of a face-centered cubic (fcc) structure of PtNi alloy nanoparticles, resulting in expansion of the Pt-Pt bond distance;<sup>37</sup> however, the present intermetallic PtCu system showed the opposite effect. It is most likely that doped N atoms are substitutional at Cu sites, which induces the contraction in Pt-Pt bonding in Int-PtCuN/KB. This hypothesis is supported by the DFT calculations. The DFT-relaxed structure shows that with a N atom substituted at a Cu site, the local structure is stable compared with the unsubstituted case, as shown in Figure 4g and 4h. The relaxed cell parameters are shown in Table S9. A possibility of the presence of N atoms in Pt sites is unlikely, since there is no Pt-N contribution in the Pt L3-edge FT-EXAFS of Int-PtCuN/KB ((Figures 4f) and some experiments demonstrated that the formation of Pt-N bonds requires high pressures and temperatures (~ 50 GPa and 2000K).<sup>51</sup> In addition, the compressive strain

introduced by N substitution can be further confirmed via comparing the bond length of Pt-Pt in the ordered PtCu with and without N atoms in the relaxed DFT results. As displayed in Figure 4i, the shrinkage of bond length for the neighboring Pt atoms surrounding a Cu atom occurs along the basal plane when the Cu atom is substituted by a N atom, *i.e.*, the bond length of Pt-Pt is reduced from 2.74 Å to 2.71 Å, which is qualitatively in agreement with the fitting results of EXAFS. We also note that the formation of the ordered intermetallic structure generates the compressive strain in Pt bonding (Int-PtCuN/KB) compared with D-PtCuN/KB. That is to say, both the N-doping and the transformation from disordered to the ordered intermetallic phase can tune the compressive strain in the Pt atoms on the surface, and this synergistic ligand effect is likely one of the origins of the enhanced activity and stability of Int-PtCuN/KB.

The CN of Cu-N for Int-PtCuN/KB and D-PtCuN/KB are determined to be  $0.8 \pm 0.4$  and  $0.4 \pm 0.3$  (Table S6), respectively, further confirming the difference of the two PtCu structures between the disordered phase (fcc) and the ordered intermetallic L1<sub>1</sub> (R-3m rhombohedral) phase. It has been reported that some metal-nitrogen moieties, like Fe-N<sub>x</sub>, have catalytic active and chemical durable in the acidic electrolyte. S2-S4 Recently, we proposed a mechanism for the enhanced stability for the Int-PtNiN/KB catalyst, which is also considered as a plausible cause of the durability of Int-PtCuN/KB; the strong Cu-N bonding provides a pinning effect from the N atom to the coordinated Cu atoms. Moreover, the diffusivity of Cu atoms is suspended by the intermetallic structure, through the Pt planes sandwiching every Cu-N moiety plane, which greatly enhances the etching resistance for Cu atoms located in the core. We believe that the lowered diffusivity of Cu atoms through the two effects protects Cu from leaching out during the ORR process, and this is the other origin of the superb durability of the Int-PtCuN/KB catalysts.

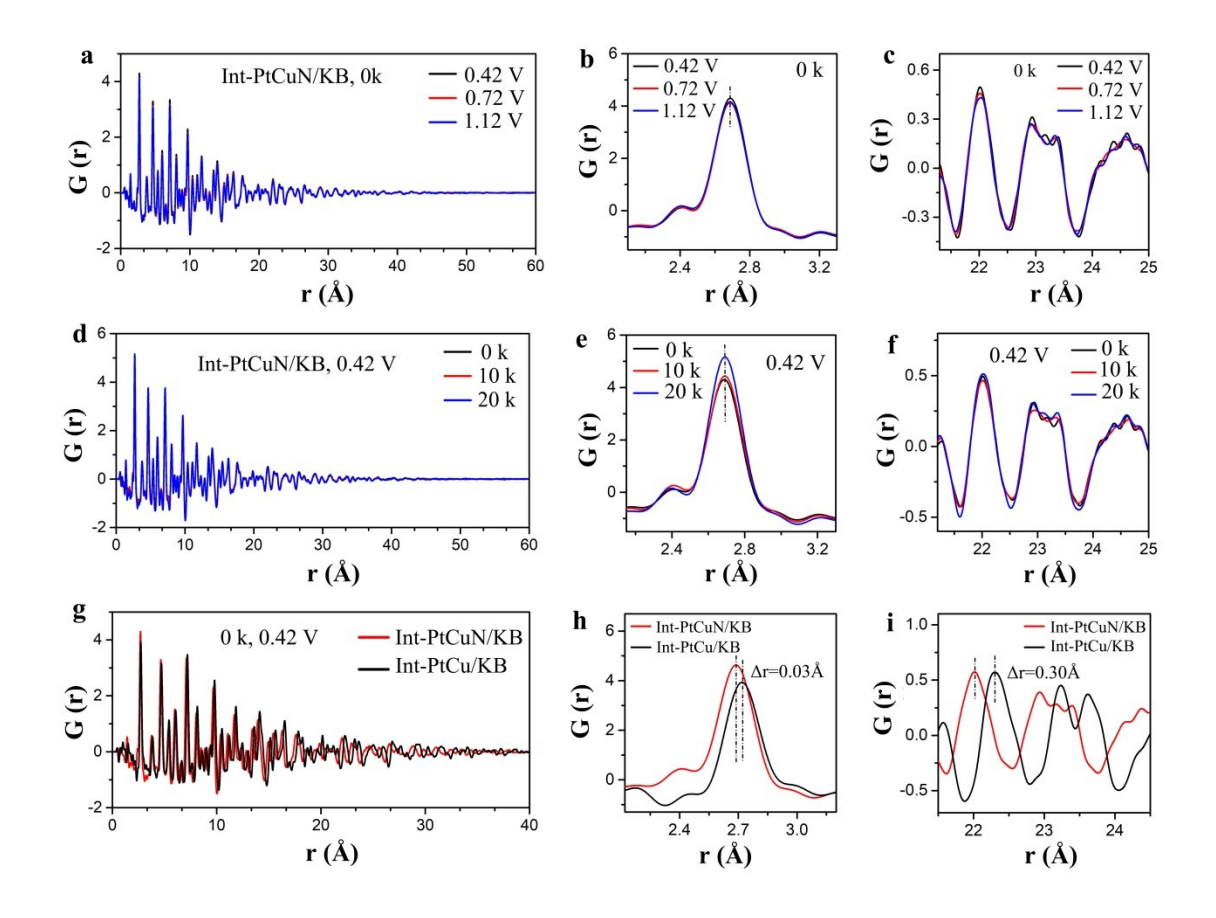


**Figure 5.** (a-c) *In situ* PDF patterns of Int-PtCuN/KB at different applied potentials. (d-f) *In situ* PDF spectra of Int-PtCuN/KB at 0.42 V after different cycle tests (0k, 10k, 20k). (g-i) *In situ* PDF patterns of Int-PtCuN/KB and Int-PtCu/KB at 0.42 V before cycle tests (0k).

Additionally, to further determine the stability of the ordered structure during the ORR process, *in situ* PDF and *in situ* XRD measurements of the ordered intermetallic catalysts were performed in a 0.1 M HClO4 electrolyte not only under various potentials but also different ADT cycles. The experimental PDFs G(r) of the Int-PtCuN/KB catalysts are shown in Figure 5, and the corresponding X-ray scattering pattern (I(q)), scattering structure function (S(q)), and reduced structure function (F(q)) are shown in Figure S11, S12, and S13, respectively. Under increasing potentials from 0.42 V to 1.12 V, the peak positions of the Int-PtCuN/KB show a negligible shift (Figure 5a-c), indicating that the N-doped and ordered structure impart an good resistance against oxidation up to a high potential of 1.12 V. Similarly, even after 20,000 ADT cycles, the characteristic peak positions of the Int-PtCuN/KB also show no obvious changes at the same potential (at 0.42 V as shown in Figure 5d-e), providing evidence that no significant dissolution occurred and the core-shell

ordered structure was maintained to a great extent. Meanwhile, the in situ XRD results of Int-PtCuN/KB and Int-PtCu/KB can further confirm the conclusion of the in situ PDF. As can be seen from Figure S14 and S15, all of the peak positions of the in situ XRD match well with the standard PDF of the ordered PtCu (PDF #42-1326), and which, whether under various potentials or different ADT cycles, exhibit almost no shift. It has been known that PDF and XRD analysis are very powerful tools for structural characterization of nanoparticles, and therefore the in situ PDF and in situ XRD results demonstrate that the ordered structure of Int-PtCuN/KB and Int-PtCu/KB are very stable during the ORR and ADT processes. As shown in Figure 5g-i and Figure S16, both the PDF and XRD peaks of the Int-PtCuN/KB shift to the lower angles than those of the Int-PtCu/KB. This observation clearly demonstrates that the Int-PtCuN/KB is contracted compared with the Int-PtCu/KB because the N dopants induce the compressive strain in Int-PtCu/KB, which is in line with the in situ XAS results. Moreover, combined with the ORR results above, it can be illustrated that the N-doping and the formation of the ordered intermetallic structure not only enhances the intrinsic activity of ORR but also improves the durability of the ordered intermetallic catalysts.

#### **Conclusions**

In conclusion, we have successfully synthesized the N-doped and rhombohedral ordered L1<sub>1</sub> Int-PtCuN/KB catalyst with superior activity and durability for the ORR. The MA and SA of the Int-PtCuN/KB improve 5.2 and 3.9 times compared to the commercial Pt/C, respectively, and even the MA loss after 20,000 ADT cycles is only 23.4 %. The *in situ* XAS and *in situ* XRD/PDF results elucidate that the enhancement of the ORR performance for Int-PtCuN/KB originates from the synergistic effect of (i) the introduction of a compressive strain through the N-doping and the formation of the rhombohedral ordered structure, which is beneficial to the adsorption of intermediates on the Pt surface, (ii) the presence of the Pt monolayer shell, which can effectively protect Cu against acid etching, and (iii) the retardation of Cu diffusivity by the Cu-N bonding and the intermetallic ordering, resulting in alleviating Cu dissolution from the core. This work provides valuable insights and

possibilities to design binary even ternary Pt-based electrocatalysts with high performance and long-term durability for the ORR through a simple and facile synthesis method.

## **Supporting Information**

The details of material synthesis and characterizations, measurements details and DFT details are provided in the Supporting Information. This information is available free of charge on the ACS Publications website.

#### Acknowledgement

This work has contributions from employees and/or guests of Brookhaven Science Associates under Contract Number DE-SC0012704 with the U.S. Department of Energy. TEM characterization/simulations and DFT calculations done by the UCI team were support by the National Science Foundation under award number CHE-1900401. R.Z. was supported by the startup funding of H.L.X. The EXAFS analysis done by AIF was supported as part of the Integrated Mesoscale Architectures for Sustainable Catalysis (IMASC), an Energy Frontier Research Center funded by the U.S. Department of Energy, Office of Science, Basic Energy Sciences under Award Number DE-SC0012573. This research made use of the Center for Functional Nanomaterials, the PDF/XPD beamline (28-ID-1/28-ID-2) and the QAS beamline (7-BM) of the National Synchrotron Light Source II, which are U.S. DOE Office of Science Facilities, at Brookhaven National Laboratory under Contract Number DE-SC0012704. The QAS beamline operations were supported in part by the Synchrotron Catalysis Consortium (U.S. DOE, Office of Basic Energy Sciences, Grant Number DE-SC0012335).

## References

- (1) Debe, M. K., Electrocatalyst Approaches and Challenges for Automotive Fuel Cells. *Nature* **2012**, *486*, 43-51.
- (2) Tian, X.; Lu, X. F.; Xia, B. Y.; Lou, X. W., Advanced Electrocatalysts for the Oxygen Reduction Reaction in Energy Conversion Technologies. *Joule* **2020**, *4*, 45-68.
- (3) Shao, M.; Chang, Q.; Dodelet, J. P.; Chenitz, R., Recent Advances in Electrocatalysts for Oxygen Reduction Reaction. *Chem. Rev.* **2016**, *116*, 3594-3657.

- (4) Stamenkovic, V. R.; Strmcnik, D.; Lopes, P. P.; Markovic, N. M., Energy and Fuels from Electrochemical Interfaces. *Nat. Mater.* **2016**, *16*, 57-69.
- (5) Liu, M.; Zhao, Z.; Duan, X.; Huang, Y., Nanoscale Structure Design for High-Performance Pt-Based ORR Catalysts. *Adv. Mater.* **2019**, *31*, 1802234.
- (6) Nie, Y.; Li, L.; Wei, Z., Recent Advancements in Pt and Pt-free Catalysts for Oxygen Reduction Reaction. *Chem. Soc. Rev.* **2015**, *44*, 2168-2201.
- (7) Lefèvre, M.; Proietti, E.; Jaouen, F.; Dodelet, J. P., Iron-Based Catalysts with Improved Oxygen Reduction Activity in Polymer Electrolyte Fuel Cells. *Science* **2009**, *324*, 71-74.
- (8) Sasaki, K.; Naohara, H.; Cai, Y.; Choi, Y. M.; Liu, P.; Vukmirovic, M. B.; Wang, J. X.; Adzic, R. R., Core-protected Platinum Monolayer Shell High-stability Electrocatalysts for Fuel-cell Cathodes. *Angew. Chem. Int. Ed.* **2010**, *49*, 8602-8607.
- (9) Kuttiyiel, K. A.; Choi, Y.; Hwang, S. M.; Park, G. G.; Yang, T. H.; Su, D.; Sasaki, K.; Liu, P.; Adzic, R. R., Enhancement of the Oxygen Reduction on Nitride Stabilized Pt-M (M=Fe, Co, and Ni) core-shell Nanoparticle Electrocatalysts. *Nano Energy* **2015**, *13*, 442-449.
- (10) Sasaki, K.; Naohara, H.; Choi, Y.; Cai, Y.; Chen, W. F.; Liu, P.; Adzic, R. R., Highly Stable Pt Monolayer on PdAu Nanoparticle Electrocatalysts for the Oxygen Reduction Reaction. *Nat. Commun.* **2012,** *3*, 1115.
- (11) Wang, J. X.; Inada, H.; Wu, L.; Zhu, Y.; Choi, Y.; Liu, P.; Zhou, W. P.; Adzic, R. R., Oxygen Reduction on Well-Defined Core-Shell Nanocatalysts: Particle Size, Facet, and Pt Shell Thickness Effects. *J. Am. Chem. Soc.* **2009**, *131*, 17298-17302.
- (12) Chung, D. Y.; Jun, S. W.; Yoon, G.; Kwon, S. G.; Shin, D. Y.; Seo, P.; Yoo, J. M.; Shin, H.; Chung, Y. H.; Kim, H.; Mun, B. S.; Lee, K. S.; Lee, N. S.; Yoo, S. J.; Lim, D. H.; Kang, K.; Sung, Y. E.; Hyeon, T., Highly Durable and Active PtFe Nanocatalyst for Electrochemical Oxygen Reduction Reaction. *J. Am. Chem. Soc.* 2015, 137, 15478-15485.
- (13) Strasser, P.; Koh, S.; Anniyev, T.; Greeley, J.; More, K.; Yu, C.; Liu, Z.; Kaya, S.; Nordlund, D.; Ogasawara, H.; Toney, M. F.; Nilsson, A., Lattice-strain Control of the Activity in Dealloyed Core-shell Fuel Cell Catalysts. *Nat. Chem.* **2010**, *2*, 454-460.
- (14) Mani, P.; Srivastava, R.; Strasser, P., Dealloyed Binary PtM<sub>3</sub> (M=Cu, Co, Ni) and Ternary PtNi<sub>3</sub>M (M=Cu, Co, Fe, Cr) Electrocatalysts for the Oxygen Reduction Reaction: Performance in Polymer Electrolyte Membrane Fuel Cells. *J. Power Sources* **2011**, *196*, 666-673.

- (15) Lim, B.; Jiang, M.; Camargo, P. H. C.; Cho, E. C.; Tao, J.; Lu, M.; Zhu, Y.; Xia, Y., Pd-Pt Bimetallic Nanodendrites with High Activity for Oxygen Reduction. *Science* **2009**, *324*, 1302-1305.
- (16) Gong, M.; Deng, Z.; Xiao, D.; Han, L.; Zhao, T.; Lu, Y.; Shen, T.; Liu, X.; Lin, R.; Huang, T.; Zhou, G.; Xin, H.; Wang, D., One-Nanometer-Thick Pt<sub>3</sub>Ni Bimetallic Alloy Nanowires Advanced Oxygen Reduction Reaction: Integrating Multiple Advantages into One Catalyst. *ACS Catal.* **2019**, *9*, 4488-4494.
- (17) Cui, C.; Gan, L.; Li, H. H.; Yu, S. H.; Heggen, M.; Strasser, P., Octahedral PtNi Nanoparticle Catalysts: Exceptional Oxygen Reduction Activity by Tuning the Alloy Particle Surface Composition. *Nano Lett.* **2012**, *12*, 5885-5889.
- (18) Li, J.; Sharma, S.; Liu, X.; Pan, Y.-T.; Spendelow, J. S.; Chi, M.; Jia, Y.; Zhang, P.; Cullen, D. A.; Xi, Z.; Lin, H.; Yin, Z.; Shen, B.; Muzzio, M.; Yu, C.; Kim, Y. S.; Peterson, A. A.; More, K. L.; Zhu, H.; Sun, S., Hard-Magnet L1<sub>0</sub>-CoPt Nanoparticles Advance Fuel Cell Catalysis. *Joule* **2019**, *3*, 124-135.
- (19) Xiong, Y.; Xiao, L.; Yang, Y.; DiSalvo, F. J.; Abruña, H. D., High-Loading Intermetallic Pt<sub>3</sub>Co/C Core-Shell Nanoparticles as Enhanced Activity Electrocatalysts toward the Oxygen Reduction Reaction (ORR). *Chem. Mater.* **2018**, *30*, 1532-1539.
- (20) Li, J.; Xi, Z.; Pan, Y. T.; Spendelow, J. S.; Duchesne, P. N.; Su, D.; Li, Q.; Yu, C.; Yin, Z.; Shen, B.; Kim, Y. S.; Zhang, P.; Sun, S., Fe Stabilization by Intermetallic L1<sub>0</sub>-FePt and Pt Catalysis Enhancement in L1<sub>0</sub>-FePt/Pt Nanoparticles for Efficient Oxygen Reduction Reaction in Fuel Cells. *J. Am. Chem. Soc.* **2018**, *140*, 2926-2932.
- (21) Yoo, T. Y.; Yoo, J. M.; Sinha, A. K.; Bootharaju, M. S.; Jung, E.; Lee, H. S.; Lee, B.-H.; Kim, J.; Antink, W. H.; Kim, Y. M.; Lee, J.; Lee, E.; Lee, D. W.; Cho, S.-P.; Yoo, S. J.; Sung, Y.-E.; Hyeon, T., Direct Synthesis of Intermetallic Platinum-Alloy Nanoparticles Highly Loaded on Carbon Supports for Efficient Electrocatalysis. *J. Am. Chem. Soc.* **2020**, *142*, 14190-14200.
- (22) Kim, H. Y.; Joo, S. H., Recent Advances in Nanostructured Intermetallic Electrocatalysts for Renewable Energy Conversion Reactions. *J. Mater. Chem. A* **2020**, *8*, 8195-8217.
- (23) Hu, Y.; Shen, T.; Zhao, X.; Zhang, J.; Lu, Y.; Shen, J.; Lu, S.; Tu, Z.; Xin, H. L.; Wang, D., Combining Structurally Ordered Intermetallics with N-doped Carbon Confinement for Efficient and Anti-poisoning Electrocatalysis. *Appl. Catal. B* **2020**, *279*, 119370.
- (24) Kim, H. Y.; Kim, J. M.; Ha, Y.; Woo, J.; Byun, A.; Shin, T. J.; Park, K. H.; Jeong, H. Y.; Kim, H.; Kim, J. Y.; Joo, S. H., Activity Origin and Multifunctionality of Pt-Based Intermetallic Nanostructures for Efficient Electrocatalysis. *ACS Catal.* **2019**, *9*, 11242-11254.

- (25) Liu, M.; Xin, H.; Wu, Q., Unusual Strain Effect of a Pt-based L1<sub>0</sub> Face-centered Tetragonal Core in Core/shell Nanoparticles for the Oxygen Reduction Reaction. *Phys. Chem. Chem. Phys.* **2019**, *21*, 6477-6484.
- (26) Wang, X. X.; Hwang, S.; Pan, Y.-T.; Chen, K.; He, Y.; Karakalos, S.; Zhang, H.; Spendelow, J. S.; Su, D.; Wu, G., Ordered Pt<sub>3</sub>Co Intermetallic Nanoparticles Derived from Metal-Organic Frameworks for Oxygen Reduction. *Nano Lett.* **2018**, *18*, 4163-4171.
- (27) Ma, Z.; Cano, Z. P.; Yu, A.; Chen, Z.; Jiang, G.; Fu, X.; Yang, L.; Wu, T.; Bai, Z.; Lu, J., Enhancing Oxygen Reduction Activity of Pt-based Electrocatalysts: from Theoretical Mechanisms to Practical Methods. *Angew. Chem. Int. Ed.* **2020**, *59*, 2-17.
- (28) Qin, Y.; Luo, M.; Sun, Y.; Li, C.; Huang, B.; Yang, Y.; Li, Y.; Wang, L.; Guo, S., Intermetallic hcp-PtBi/fcc-Pt Core/Shell Nanoplates Enable Efficient Bifunctional Oxygen Reduction and Methanol Oxidation Electrocatalysis. *ACS Catal.* **2018**, *8*, 5581-5590.
- (29) Rößner, L.; Armbrüster, M., Electrochemical Energy Conversion on Intermetallic Compounds: A Review. *ACS Catal.* **2019**, *9*, 2018-2062.
- (30) Xiao, W.; Lei, W.; Gong, M.; Xin, H. L.; Wang, D., Recent Advances of Structurally Ordered Intermetallic Nanoparticles for Electrocatalysis. *ACS Catal.* **2018**, *8*, 3237-3256.
- (31) Alloyeau, D.; Ricolleau, C.; Mottet, C.; Oikawa, T.; Langlois, C.; Le Bouar, Y.; Braidy, N.; Loiseau, A., Size and Shape Effects on the Order-Disorder Phase Transition in CoPt Nanoparticles. *Nat. Mater.* **2009**, *8*, 940-946.
- (32) Bu, L.; Zhang, N.; Guo, S.; Zhang, X.; Li, J.; Yao, J.; Wu, T.; Lu, G.; Ma, J. Y.; Su, D.; Huang, X., Biaxially Strained PtPb/Pt Core/shell Nanoplate Boosts Oxygen Reduction Catalysis. *Science* **2016**, *354*, 1410-1413.
- (33) Wang, D.; Xin, H. L.; Hovden, R.; Wang, H.; Yu, Y.; Muller, D. A.; DiSalvo, F. J.; Abruña H. D., Structurally Ordered Intermetallic Platinum-cobalt Core-shell Nanoparticles with Enhanced Activity and Stability as Oxygen Reduction Electrocatalysts. *Nat. Mater.* **2013**, *12*, 81-87.
- (34) Cui, Z.; Chen, H.; Zhou, W.; Zhao, M.; DiSalvo, F. J., Structurally Ordered Pt<sub>3</sub>Cr as Oxygen Reduction Electrocatalyst: Ordering Control and Origin of Enhanced Stability. *Chem. Mater.* **2015**, *27*, 7538-7545.
- (35) Gong, M.; Zhu, J.; Liu, M.; Liu, P.; Deng, Z.; Shen, T.; Zhao, T.; Lin, R.; Lu, Y.; Yang, S.; Liang, Z.; Bak, S. M.; Stavitski, E.; Wu, Q.; Adzic, R. R.; Xin, H. L.; Wang, D., Optimizing PtFe Intermetallics for

- Oxygen Reduction Reaction: from DFT Screening to in situ XAFS Characterization. *Nanoscale* **2019**, *11*, 20301-20306.
- (36) Kuttiyiel, K. A.; Sasaki, K.; Choi, Y.; Su, D.; Liu, P.; Adzic, R. R., Nitride Stabilized PtNi Core-shell Nanocatalyst for High Oxygen Reduction Activity. *Nano Lett.* **2012**, *12*, 6266-6271.
- (37) Zhao, X.; Xi, C.; Zhang, R.; Song, L.; Wang, C.; Spendelow, J. S.; Frenkel, A. I.; Yang, J.; Xin, H. L.; Sasaki, K., High-Performance Nitrogen-doped Intermetallic PtNi Catalyst for the Oxygen Reduction Reaction. *ACS Catal.* **2020**, *10*, 10637-10645.
- (38) Zhang, S.; Qi, W.; Huang, B., Size Effect on Order-disorder Transition Kinetics of FePt Nanoparticles. *J. Chem. Phys.* **2014**, *140*, 044328.
- (39) Wang, Q.; Zhao, Z. L.; Zhang, Z.; Feng, T.; Zhong, R.; Xu, H.; Pantelides, S. T.; Gu, M., Sub-3 nm Intermetallic Ordered Pt<sub>3</sub>In Clusters for Oxygen Reduction Reaction. *Adv. Sci.* **2019**, 1901279.
- (40) Kim, H. Y.; Kwon, T.; Ha, Y.; Jun, M.; Baik, H.; Jeong, H. Y.; Kim, H.; Lee, K.; Joo, S. H., Intermetallic PtCu Nanoframes as Efficient Oxygen Reduction Electrocatalysts. *Nano Lett.* **2020**, *20*, 7413-7421.
- (41) Gong, M.; Xiao, D.; Deng, Z.; Zhang, R.; Xia, W.; Zhao, T.; Liu, X.; Shen, T.; Hu, Y.; Lu, Y.; Zhao, X.; Xin, H.; Wang, D., Structure Evolution of PtCu Nanoframes from Disordered to Ordered for the Oxygen Reduction Reaction. *Appl. Catal. B* **2021**, *282*, 119617.
- (42) van der Vliet, D. F.; Wang, C.; Li, D.; Paulikas, A. P.; Greeley, J.; Rankin, R. B.; Strmcnik, D.; Tripkovic, D.; Markovic, N. M.; Stamenkovic, V. R. Unique Electrochemical Adsorption Properties of Pt-skin Surfaces. *Angew. Chem. Int. Ed.* **2012**, *51*, 3139-3142.
- (43) Ghosh, T.; Miomir, B. V.; DiSalvo, F. J.; Adzic, R. R., Intermetallics as Novel Supports for Pt Monolayer O<sub>2</sub> Reduction Electrocatalysts: Potential for Significantly Improving Properties. *J. Am. Chem. Soc.* **2010**, *132*, 906-907.
- (44) Sasaki, K.; Marinkovic, N.; Isaacs, H. S.; Adzic, R. R., Synchrotron-Based In Situ Characterization of Carbon-Supported Platinum and Platinum Monolayer Electrocatalysts. *ACS Catal.* **2016**, *6*, 69-76.
- (45) Lytle, F. W.; Wei, P. S. P.; Greegor, R. B.; Via, G. H.; Sinfelt, J. H., Effect of Chemical Environment on Magnitude of X-ray Absorption Resonance at *L<sub>III</sub>* edges. Studies on Metallic Elements, Compounds, and Catalysts. *J. Chem. Phy.* **1979**, *70*, 4849-4855.
- (46) Horsley, J. A., Relationship between the Area of  $L_{2,3}$  x-ray Absorption Edge Resonances and the d Orbital Occupancy in Compounds of Platinum and Iridium. J. Chem. Phys. 1982, 76, 1451-1458.

- (47) Frenkel, A. I., Applications of Extended X-ray Absorption Fine-structure Spectroscopy to Studies of Bimetallic Nanoparticle Catalysts. *Chem. Soc. Rev.* **2012**, *41*, 8163-8178.
- (48) Frenkel, A. I.; Wang, Q.; Sanchez, S. I.; Small, M. W.; Nuzzo, R. G., Short Range Order in Bimetallic Nanoalloys: An Extended X-ray Absorption Fine Structure Study. *J. Chem. Phys.* **2013**, *138*, 064202.
- (49) Sasaki, K.; Wang, J. X.; Naohara, H.; Marinkovic, N.; More, K.; Inada, H.; Adzic, R. R., Recent Advances in Platinum Monolayer Electrocatalysts for Oxygen Reduction Reaction: Scale-up Synthesis, Structure and Activity of Pt Shells on Pd Cores. *Electrochim. Acta* **2010**, *55*, 2645-2652.
- (50) Song, L.; Cai, Y.; Zhao, X.; Liu, Y.; Kuttiyiel, K.; Marinkovic, N.; Frenkel A.; Kim Y. S.; Kongkanand, A.; Choi Y.; Adzic, R. R.; Sasaki, K. One-step Anythesis of Highly Efficient Nitride-stabilized PtNiN Catalyst for the Oxygen Reduction Reaction, in preparation.
- (51) Crowhurst, J. C.; Goncharov, A. F.; Sadigh, B.; Evans, C. L.; Morrall, P. G.; Ferreira, J. L.; Nelson, A. J., Synthesis and Characterization of the Nitrides of Platinum and Iridium. *Science* **2006**, *311*, 1275-1278.
- (52) Tylus, U.; Jia, Q.; Strickland, K.; Ramaswamy, N.; Serov, A.; Atanassov P.; Mukerjee, S. Elucidating Oxygen Reduction Active Sites in Pyrolyzed Metal-Nitrogen Coordinated Non-Precious-Metal Electrocatalyst Systems, *J. Phys. Chem. C* **2014**,*118*, 8999-9008.
- (53) Holby E. F.; Zelenay, P. Linking Structure to Function: The Search for Active Sites in Non-platinum Group Metal Oxygen Reduction Reaction Catalysts, *Nano Energy* **2016**, *29*, 54-64.
- (54) Serov, A.; Artyushkova K.; Atanassov, P. Fe-N-C Oxygen Reduction Fuel Cell Catalyst Derived from Carbendazim: Synthesis, Structure, and Reactivity, *Adv. Energy Mater.* **2014**, *4*, 1301735.

# TOC

